DOI: 10.1002/chem.200601425

VIP

Description of the Ground-State Covalencies of the Bis(dithiolato) Transition-Metal Complexes from X-ray Absorption Spectroscopy and Time-Dependent Density-Functional Calculations

Kallol Ray,[a] Serena DeBeer George,[c] Edward I. Solomon,[d] Karl Wieghardt,*[a] and Frank Neese*[b]

Abstract: The electronic structures of $[M(L^{Bu})_2]^-$ (L^{Bu} = 3,5-di-*tert*-butyl-1,2-benzenedithiol; M = Ni, Pd, Pt, Cu, Co, Au) complexes and their electrochemically generated oxidized and reduced forms have been investigated by using sulfur K-edge as well as metal K- and L-edge X-ray absorption spectroscopy. The electronic structure content of the sulfur K-edge spectra was determined through detailed comparison of experimental and theoretically calculated spectra. The calculations were based on a new simplified scheme based on quasi-relativistic time-dependent density functional theory (TD-DFT) and proved to be successful in the interpretation of the experimental data. It is shown that dithiolene ligands act as noninnocent ligands that are readily oxidized to the dithiosemiquinonate(−) forms. The extent of electron transfer strongly depends on the effective nuclear charge of the central metal, which in turn is influenced by its formal oxidation state, its position in the periodic table, and scalar relativistic effects for the heavier metals. Thus, the complexes $[M(L^{Bu})_2]^-$ (M = Ni, Pd, Pt) and $[Au(L^{Bu})_2]$ are best described as delocalized class III mixed-valence ligand radicals bound to low-spin d^8 central metal ions while $[M(L^{Bu})_2]^-$ (M = Cu, Au) and $[M(L^{Bu})_2]^{2-}$ (M = Ni, Pd, Pt) contain completely reduced dithiolato(2−) ligands. The case of $[Co(L^{Bu})_2]^-$ remains ambiguous. On the methodological side, the calculation led to the new result that the transition dipole moment integral is noticeably different for $S_{1s}\rightarrow$valence-π versus $S_{1s}\rightarrow$valence-σ transitions, which is explained on the basis of the differences in radial distortion that accompany chemical bond formation. This is of importance in determining experimental covalencies for complexes with highly covalent metal–sulfur bonds from ligand K-edge absorption spectroscopy.

Keywords: density functional calculations · dithiolenes · S ligands · transition metals · X-ray absorption spectroscopy

Introduction

Transition-metal dithiolenes play important roles in the catalysis of a variety of formal oxygen-transfer reactions at the active sites of pyranopterin molybdenum and tungsten enzymes[1] and in specific model systems.[2] Understanding the enzymatic reaction mechanisms or design of new functional materials should be based on a thorough understanding of

[a] Dr. K. Ray, Prof. Dr. K. Wieghardt
Max-Planck-Institut für Bioanorganische Chemie
Stiftstrasse 34–36, 45470 Mülheim an der Ruhr (Germany)
Fax: (+49) 208-3063951
E-mail: wieghardt@mpi-muelheim.mpg.de

[b] Prof. Dr. F. Neese
Institut für Physikalische und Theoretische Chemie
Wegelerstr. 12, 53115 Bonn (Germany)
Fax: (+49) 228-739064
E-mail: neese@thch.uni-bonn.de

[c] Dr. S. DeBeer George
Stanford Synchrotron Radiation Laboratory, SLAC
Stanford University, Stanford, CA, 94309 (USA)

[d] Prof. Dr. E. I. Solomon
Department of Chemistry
Stanford University, Stanford, CA 94305 (USA)

Supporting information for this article is available on the WWW under http://www.chemeurj.org/ or from the author. Figure S1 shows the comparison of the S K-edge data for $[Ni(L^{Bu})_2]^{2-}$, $[Pd(L^{Bu})_2]^{2-}$, and $[Pt(L^{Bu})_2]^{2-}$. Figure S2 shows a comparison of the normalized Pt L_3-edges of the $[Pt(L^{Bu})_2]^-$ and $[Pt(L^{Bu})_2]^{2-}$ complexes. Figure S3 shows the Cu K-edge data on $[Cu(L^{Bu})_2]^-$. Figure S4 shows the Co K- and L-edges on $[Co(L^{Bu})_2]^-$. Table S1 lists the composition of important orbitals in $[M(L^{Bu})_2]^z$ complexes as obtained from DFT calculations.

the electronic structures of the active sites of the bioenzymes. Consequently, a large number of transition-metal dithiolene complexes have been synthesized and subjected to detailed physical characterizations.[3]

The most characteristic feature of transition-metal dithiolene complexes derived from d^{1-9} metals is the existence of an electron-transfer series, the members of which are interrelated by reversible one-electron steps.[3] Initial developments in the dithiolene field, which have been summarized by McCleverty,[3b] led to the recognition and experimental realization of the three-membered, planar series as shown in Scheme 1, with M = Ni, Pd or Pt, in which the terminal

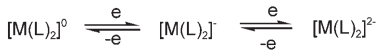

Scheme 1.

members are diamagnetic and the monoanion has an $S = 1/2$ ground state. In this series L^{2-} represents the benzene-1,2-dithiolato ligand. Mono- and dicationic members of a five-membered[3b] series are conjecturable, with the latter involving M^{II} bound to two ligands in the 1,2-dithiobenzoquinone form. However, no species of the types $[M(L)_2]^{1+,2+}$ have been detected so far.

The known ambiguities in the limiting descriptions of the metal and ligand oxidation states are summarized in Scheme 2. While the structural and electronic properties of the dianions are consistent with the indicated M^{II}–dithiolate description, the ground states of the monoanion and the neutral complexes pose intriguing electronic structure problems. The $[M(L)_2]^-$ and the related $[M(L^{Me})_2]^-$ and $[M(L^{Bu})_2]^-$ complexes have been interpreted differently in terms of the presence of a M^{III} ion bound to two dithiolato(2−) ligands[4] or a M^{II} ion bound to both the dithiolato(2−) and dithiobenzosemiquinonato(−) forms of the ligand.[5] Here L^{Me} and L^{Bu} refer to commercially available 4-methyl-1,2-benzenedithiol and Sellmann's[6] 3,5-di-*tert*-butyl-1,2-benzenedithiol ligands, respectively. The neutral complex can also be formulated in at least three different ways (Scheme 2). Possibility **I** would feature a high valent central metal ion and is the formulation preferred by Sellmann and co-workers in similar complexes.[4a] Formulation **II** corresponds to the formulation of Gray et al.[7] in a series of related compounds and favors a diradical formulation, while formulation **III** corresponds to Holm's suggestion[8] and is based on ionic resonance structures involving dithiobenzoquinone and benzene-1,2-dithiolate(2−) forms of the ligands. Density functional calculations for related compounds, though similar in outcome, have been interpreted differently in favour of one alternative or the other.[9,10]

Proper determination of the electronic structure of the transition-metal dithiolene complexes requires identification of structural and spectroscopic features that allow the unequivocal detection and characterization of dithiobenzosemiquinonate(−) radical ions in coordination complexes. Many authors[11,12] have attempted to discern between a dithiolato(2−) and its monoanionic radical form in a given complex by their crystallographically determined structural parameters. The underlying assumption has always been that the phenyl ring has either six equidistant C–C bonds in a thiolate or displays a quinoidal distortion with two alternating shorter C=C bonds and four longer ones in the radical form and, in addition, the C–S bonds were assumed to shrink upon oxidation of a dianionic thiolate to a monoanionic radical. This behavior had been firmly established for the corresponding complexes that contain catecholates and semiquinonates.[13] This is, in part, a misconception for the sulfur analogues. The structures of the phenoxyl and thiyl radicals have been calculated by theoretical methods.[14,15] The results show that the expected structural changes in comparison with their closed-shell phenolate and

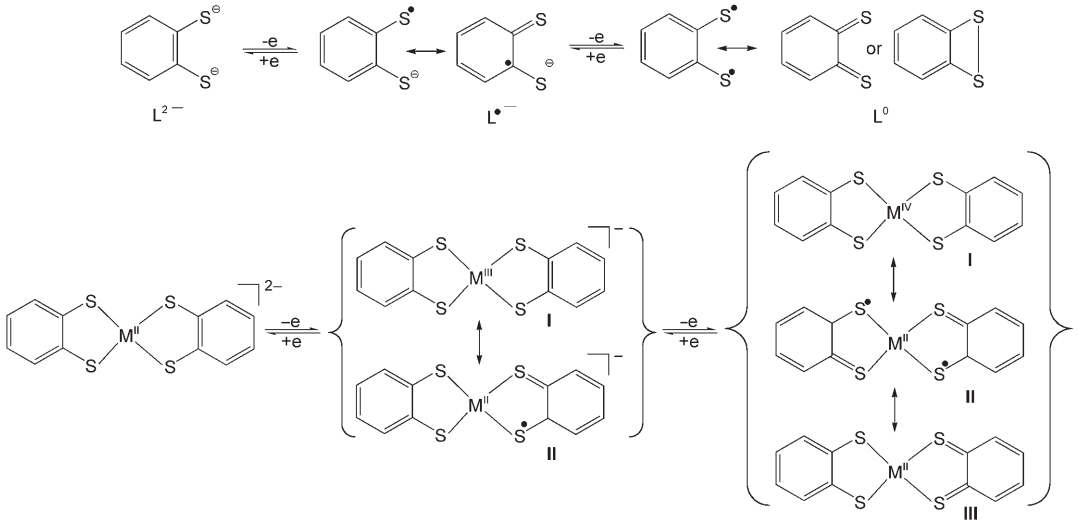

Scheme 2. The three oxidation levels of benzene-1,2-dithiol ligand and depictions of the limiting ligand and metal oxidation levels for planar members of the electron transfer series $[M(L)_2]^{0,-,2-}$.

thiophenolate forms are only observed for the phenoxyl but not the thiyl radicals. This observation is due to the fact that the spin-density distribution of the radicals differs. In the phenoxyl moiety only 38% of the spin density resides on the oxygen atom, 24% is found at each of the two *ortho*-carbon atoms, and 32% is at the *para*-carbon. In contrast, in the thiyl radical 68% of the spin density resides at the sulfur atom and only 32% is delocalized over the *ortho*- and *para*-positions of the phenyl ring. Consequently, the six C–C distances in a thiyl radical more closely resemble those of the aromatic thiolate analogue, but the C–S bond is slightly shorter at 1.75 Å. Therefore, structural parameters may be of only limited value for the identification of the redox state of benzene-1,2-dithiolate ligands in a given complex.

The problem of correctly understanding the electronic structure of the ground state of the transition-metal dithiolenes is thus a nontrivial problem and insights from sophisticated experiments are a prerequisite for progress in the field. In particular, the ground-state formulation has a bearing on the reactivity of such complexes, since Stiefel and coworkers have found that similar compounds can selectively and reversibly bind olefins[16] with potentially large impact on industrial olefin separation processes. Clearly, the question whether ligand radicals persist in such complexes or not is at the heart of the formulation of a correct reaction mechanism.

In a series of previous publications[15b,17,10] from our group we have elucidated in detail the electronic structures of the transition-metal dithiolenes involving the $(L)^{2-}$, $(L^{Bu})^{2-}$ and $(L^{Me})^{2-}$ ligands by experimental, DFT, and correlated ab initio methods. It has been shown that the ligands in such complexes readily undergo one-electron oxidation, yielding S,S′-coordinated dithiobenzosemiquinonato (S-centred) radical (−) monoanions ($L^{\bullet-}$, $L^{Bu\bullet-}$, or $L^{Me\bullet-}$). Spectroscopic markers for such radical ions have been assigned as follows: 1) presence of intense ligand-to-ligand charge-transfer bands in the near infrared region and 2) for complexes involving the L^{Bu} ligands, an intense IR band at $\approx 1100\ cm^{-1}$.

Quantum chemical studies[17d] have also been performed to analyze the origin of the IR band at $\approx 1100\ cm^{-1}$. The results show that the band originates from a C–S stretch; however, the IR intensities have to be viewed with caution, since they strongly depend on substituent effects, and the intensity mechanism is indirect. In contrast, the corresponding totally symmetric resonance Raman band, also observed at $\approx 1100\ cm^{-1}$, is found to have an electronic origin related to radical character of the dithiolene ligands, and hence provides a reliable vibrational indicator of the open shell character. However, it is still important to obtain insight into the electronic structure of dithiolenes from more direct experimental probes of open-shell character. In this respect, ligand K-edge X-ray absorption spectroscopy (XAS) is an ideal experimental method for probing the radical character of the transition-metal dithiolenes.[18,19] In the case of sulfur, a ligand K-edge results primarily from an electric dipole allowed S 1s→4p transition, the energy of which will depend on the effective nuclear charge on the sulfur. At lower energy additional features may occur that correspond to transitions to unoccupied antibonding orbitals with sulfur 3p character. In transition-metal sulfur complexes, pre-edge features are observed, which correspond to transitions to molecular orbitals formed by metal-3d–ligand-3p interactions. The intensity of the pre-edge features depends on the extent of 3p mixing, and thus can be used as a measure of covalency.[20] This method has been used extensively to obtain insight into the sulfur-ligated active sites in blue copper proteins, CuA, Fe–S proteins, and NiSOD (SOD = super oxide dismutase).[21] It has also been applied to numerous model systems, including $[Ni(Me_2C_2S_2)_2]^{2-/-/0}$ complexes.[10] These studies showed that the acceptor orbitals of the $[Ni(Me_2C_2S_2)_2]^{2-/-/0}$ series possess greater than 50% sulfur character. Therefore, the bonding description is said to be "inverted", with dithiolene valence orbitals lying at higher energy than the Ni d-orbital manifold. This exemplifies the noninnocent behavior of dithiolene ligands in many metallodithiolene complexes.

In this work, an extensive combined experimental XAS and DFT study of a series of bis(dithiolene) complexes is reported in order to obtain direct insight into the sulfur-radical character of the systems under investigation. In addition to sulfur K-edge XAS, we have also performed a number of measurements on various metal edges to substantiate the conclusions drawn from the sulfur K-edges. In interpreting the experimental results we have made use of a new, simple but nevertheless effective DFT-based technique, which allowed the direct calculation of the sulfur K-pre-edge region of the XAS spectra. In general, the agreement between theory and experiment is excellent and greatly aided in the quantitative interpretation of the experiments in terms of metal–ligand covalencies and open-shell character. Thus, the present study complements our previous combined experimental and theoretical efforts to obtain insight into the nature of metal–radical interactions in coordination compounds,[10,15b,17,22] and adds the dimension of XAS spectroscopy to the previously employed arsenal of experimental techniques.

Experimental Section

Sample preparation: The $[M(L^{Bu})_2]^-$ (M = Ni, Pd, Pt, Cu, Co, Au) and the neutral $[Au(L^{Bu})_2]$ complexes were synthesized as described in references [15b] and [17]. The neutral $[M(L^{Bu})_2]$ (M = Ni, Pd, Pt) complexes were generated electrochemically by one-electron oxidation at a controlled, fixed potential of +0.2 V versus Fc^+/Fc at −25 °C of a solution containing the corresponding monoanionic $[M(L^{Bu})_2]^-$ (M = Ni, Pd, Pt) complexes in 1.5 mM concentration in CH_2Cl_2 (5 mL; 0.10 M $[N(n\text{Bu})_4]PF_6$). The $[M(L^{Bu})_2]^{2-}$ (M = Ni, Pd, Pt) complexes were also generated electrochemically by one-electron reduction at a controlled, fixed potential of −1.2 V versus Fc^+/Fc at −25 °C of a solution containing the corresponding monoanionic $[M(L^{Bu})_2]^-$ (M = Ni, Pd, Pt) complexes in 1.5 mM concentration in CH_2Cl_2 (5 mL; 0.10 M $[N(n\text{Bu})_4]PF_6$) under totally anaerobic conditions.

All monoanionic forms of the Au, Ni, Pd, Pt, Co, and Cu complexes (and the neutral Au complex) were run as both solids and as solution in dichloromethane. In all cases the solid and solution data were essentially

identical, and here only the data on the solid monoanionic complexes are presented. For the $[M(L^{Bu})_2]^{2-}$ and $[M(L^{Bu})_2]$ (M = Ni, Pd, Pt) complexes, spectra in CH_2Cl_2 are reported. For the S and metal K-edges (Co, Ni, Cu) and metal L-edges (Au and Pt) XAS measurements the concentrations were ≈1.5 mM. Samples were loaded in an inert atmosphere glove box and immediately frozen in liquid nitrogen. Samples were maintained at temperatures of −60 °C or lower (for S K-edges) and 10 K for all metal K-edge (Co, Ni, Cu) and L-edge (Au, Pt) measurements. Co, Ni, and Cu L-edge measurements were made only on the monoanionic complexes as solids.

X-ray absorption spectroscopy and measurements and data analysis: All data were measured at the Stanford Synchrotron Radiation Laboratory under ring conditions of 3.0 GeV and 60–100 mA. All S K-edge data were measured by using the 54-pole wiggler beam line 6-2 in high magnetic field mode of 10 kG with a Ni-coated harmonic rejection mirror and a fully tuned Si(111) double crystal monochromator. Details of the optimization of this setup for low-energy studies have been described previously.[23] All solid samples were measured at room temperature as fluorescence spectra. Samples were ground finely and dispersed as thinly as possible on Mylar tape to minimize the possibility of self absorption effects. Solution samples were loaded by mans of a syringe into an aluminum block with a 6-μm-thick polypropylene window and measured at −60 to −90 °C using fluorescence detection. Data represent 2–6 scan averages. All samples were monitored for photoreduction throughout the course of data collection. The energy was calibrated from S K-edge spectra of $Na_2S_2O_3 \cdot 5H_2O$, run at intervals between sample scans. The maximum of the first pre-edge feature in the spectrum was fixed at 2472.02 eV. A step size of 0.08 eV was used over the edge region. Data were averaged, and a smooth background was removed from all spectra by fitting a polynomial to the pre-edge region and subtracting this polynomial from the entire spectrum. Normalization of the data was accomplished by fitting a flattened polynomial or straight line to the post-edge region (2490–2740 eV) and normalizing the post-edge to 1.0.

Co, Ni, and Cu L-edge data were measured by using the 31-pole wiggler beam line 10-1 by using a spherical grating monochromator set at 1000 lines mm^{-1} with 20–40 μm entrance and exit slits. Samples were finely ground and spread across double-adhesive conductive carbon tape, which was attached to either an aluminum (for Cu samples) or a copper (Co and Ni samples) paddle. The data were measured at room temperature as total electron yield spectra utilizing a Galileo 4716 channeltron electron multiplier as a detector. Three to four scans were measured in order to check reproducibility; the presented data represent a single scan. $CoCO_3$, NiF_2, and CuF_2 spectra were used as energy calibration and were run at intervals between Co, Ni, and Cu sample scans, respectively. The maximum of the L_3 edges were assigned as follows: 779.3 eV for $CoCO_3$, 852.7 eV for NiF_2, and 930.5 eV for CuF_2. In all cases, a linear background was fit to the pre-edge region and was subtracted from the entire spectrum. Normalization was accomplished by fitting a straight line to the post-edge region and normalizing the edge jump to 1.0.

Co, Ni, and Cu K-edge and Au and Pt L_3 XAS data were measured on unfocused bend magnet beam line 2-3 or focused 16-pole wiggler beam line 9-3. A Si (220) monochromator was utilized for energy selection. The monochromator was detuned 50% (for beam line 2-3) to minimize higher harmonic components in the X-ray beam (for beam line 9-3 a harmonic rejection mirror was present). All solid samples were prepared as dilute matrix in boron nitride, pressed into a pellet and sealed between 38 μm Kapton tape windows in a 1 mm aluminum spacer. Solution samples were loaded into 1 mm Lucite XAS cells with 6 μm polypropylene windows and then frozen immediately by immersion in liquid nitrogen prior to data collection. Samples were maintained at 10 K during data collection by using an Oxford Instruments CF1208 continuous flow liquid helium cryostat. Data were measured in the transmission mode. Internal energy calibrations were performed by simultaneous measurement of the appropriate metal reference foil placed between a second and third ionization chamber. The first inflection points were assigned to 7709.5, 8831.6, 8980.3, 11920.0, and 11563.0 eV for Co, Ni, Cu, Au, and Pt foils, respectively. Data represent two to six scan averages and were processed by fitting a second-order polynomial to the pre-edge region and subtracting this background from the entire spectrum. A three-region cubic spline was used to model the smooth background above the edge. The data were normalized by subtracting the spline and normalizing the post-edge 1.0.

Computational methods: All calculations in this work were performed with the electronic structure program ORCA.[24] The method for predicting S and Cl K-edge spectra will be described in detail in a separate publication. Briefly, the method consisted of the following elementary steps:

1) Following a ground-state DFT calculation with the BP86 functional,[27a,b] the S-1s orbitals were localized if there are several symmetry equivalent sulfur atoms in the molecules ("sudden approximation").
2) The TD-DFT equations were solved in the standard way[27c] with the slight modification that only excitations out of the localized sulfur 1 s-orbital were allowed.
3) Since the absolute calculated transition energies show large errors due to a variety of reasons including shortcomings in the treatment of relativity and shortcomings of the DFT potentials in the core-regions, it was necessary to establish a constant shift for each element studied; this shift was applied to the transition energies.

Using the combination of methods and basis sets described below a value of 61.22 eV was established for sulfur.

We carefully studied the effects of changing the basis set, functional, charge-compensation treatment, and different scalar relativistic corrections that were all implemented into the ORCA package. The protocol below turned out to be the most successful combination for the prediction of S (and Cl) K-edge spectra: The simulated spectra contained both dipole- and quadrupole contributions, and scalar relativity was included by using the ZORA method[25a] in the modification described by van Wüllen.[25b] Large uncontracted Gaussian basis sets derived from the well-tempered basis sets of Huzinaga[28] were used at the metal and sulfur centers. For the remaining atoms we used the all-electron polarized triple-ξ (TZVP)[29] Gaussian basis sets of the Ahlrichs group, but uncontracted them in order to allow for a distortion of the inner shell orbitals in the presence of the relativistic potential. Since the compounds studied in this work are mostly anions, we carried out the calculations in a dielectric continuum using the conductor like screening model (COSMO).[30] CH_2Cl_2 ($\varepsilon = 9.08$) was used as solvent. Spin unrestricted calculations were performed for all the complexes.

Experimental Results

Au complexes—S K-edges: Figure 1A shows a comparison of the S K-edge data for the monoanionic and neutral Au complexes. The S K-edge of $[Au(L^{Bu})_2]^-$ shows a single intense pre-edge peak at 2471.18 eV (with an integrated area of 1.89 units, Table 1). The S K-edge of the $[Au(L^{Bu})_2]^0$ complex clearly shows two pre-edge features, a lower energy feature at 2469.8 eV (with an area of 0.70 units) and a higher energy feature, similar to the monoanionic complex, at 2471.12 eV (with an area of 1.56 units, Table 1). The rising edge inflection point of the $[Au(L^{Bu})_2]^0$ complex is shifted 0.25 eV to higher energy than in the monanionic complex.

Au complexes—Au L-edges: Figure 1B shows a comparison of the Au L_3-edge data. The complexes show small changes in the white line and continuum structure, but the rising edge inflection points are essentially identical.

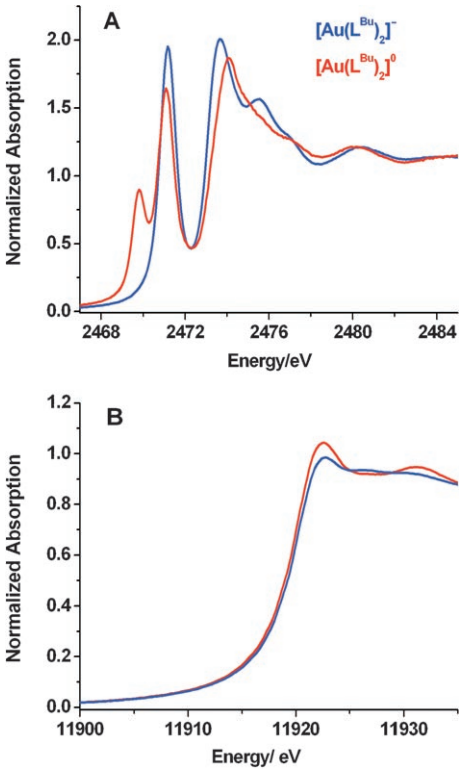

Figure 1. Comparisons of the normalized S K-edge (A) and Au L_3-edge (B) data for $[Au(L^{Bu})_2]^-$ and $[Au(L^{Bu})_2]^0$.

Table 1. Comparison of calculated and experimentally determined XAS spectra for the series of dithiolenes studied.

	Transition energies [eV] Calcd(+61.22)	Exptl	Area	Exptl oscillator strengths ($\times10^4$)[a]	Calcd oscillator strengths ($\times10^4$)[b]
$[Ni(L)_2]^-$	2469.68	2469.78	0.629	6.34	5.60
	2470.90	2470.77	1.090	11.17	12.70
$[Pd(L)_2]^-$	2469.59	2469.61	0.718	7.24	6.60
	2471.17	2471.40	1.160	11.89	13.30
$[Pt(L)_2]^-$	2469.88	2469.98	0.660	6.66	6.50
	2472.00	2472.30	1.220	12.51	11.20
$[Au(L)_2]^0$	2469.80	2469.80	0.704	7.10	7.10
	2471.18	2471.12	1.560	16.00	16.00
$[Au(L)_2]^-$	2470.83	2471.18	1.890	19.38	15.40
$[Cu(L)_2]^-$	2469.85	2470.05	1.520	15.59	17.00
$[Ni(L)_2]^{2-}$	2470.76	2470.81	0.652	6.69	10.80
$[Pd(L)_2]^{2-}$	2470.83	2471.4	[c]		11.70
$[Pt(L)_2]^{2-}$	2471.40	2472.1	[c]		10.80
$[Co(L)_2]^-$	2469.68	2470.16	0.659	6.48	6.00
	2470.06				
	2471.30	2470.77	1.161	11.90	11.50
$[Ni(S_2C_2Me_2)_2]^-$	2469.97	2470.00	0.539	5.44	5.80
	2470.98	2471.00	1.295	13.30	12.40
$[Ni(S_2C_2Me_2)_2]^{2-}$	2470.94	2471.20	1.320	13.53	10.50

[a] $[Au(L)_2]^0$ calibrated oscillator strengths. [b] Dipolar oscillator strengths. [c] Feature is not well-resolved from edge and therefore accurate areas cannot be obtained.

Ni, Pd, Pt monoanionic complexes—S K-edges: Figure 2 shows a comparison of the S K-edge data for $[Ni(L^{Bu})_2]^-$, $[Pd(L^{Bu})_2]^-$, and $[Pt(L^{Bu})_2]^-$. All three complexes clearly

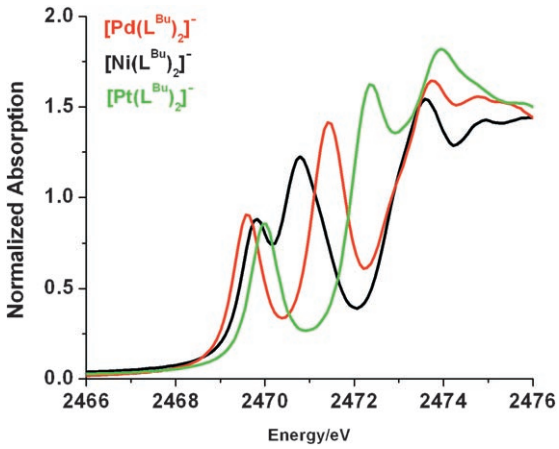

Figure 2. Comparison of the normalized S K-edge data for $[Ni(L^{Bu})_2]^-$, $[Pd(L^{Bu})_2]^-$, and $[Pt(L^{Bu})_2]^-$.

show two pre-edge features (Table 1), a weaker low-energy feature and a more intense high-energy feature. The intensity of the lowest energy feature increases slightly on going from $[Ni(L^{Bu})_2]^-$ to $[Pd(L^{Bu})_2]^-$ and then decreases slightly for the $[Pt(L^{Bu})_2]^-$ complex, while the highest energy pre-edge feature increases in intensity across the series. The transition energy of the lowest energy peak changes by less than 0.4 eV across the series, while the higher energy feature increases by $\approx$1.5 eV on going from $[Ni(L^{Bu})_2]^-$ to $[Pd(L^{Bu})_2]^-$ to $[Pt(L^{Bu})_2]^-$.

Ni, Pd, Pt dianionic complexes—S K-edges: A comparison of the S K-edge data for $[Ni(L^{Bu})_2]^{2-}$, $[Pd(L^{Bu})_2]^{2-}$, and $[Pt(L^{Bu})_2]^{2-}$ is given in Figure S1. All three complexes show only a single pre-edge feature, which increases in energy across the series, from 2470.8 to 2471.4 to 2472.1 eV for the Ni, Pd, and Pt complexes, respectively. For the Pd and Pt complexes the pre-edges are not well-resolved from the rising edge, and hence the areas are not reported.

Ni monoanionic, dianionic, and neutral complexes—S K-edges. Figure 3 gives a comparison of the S K-edge data for

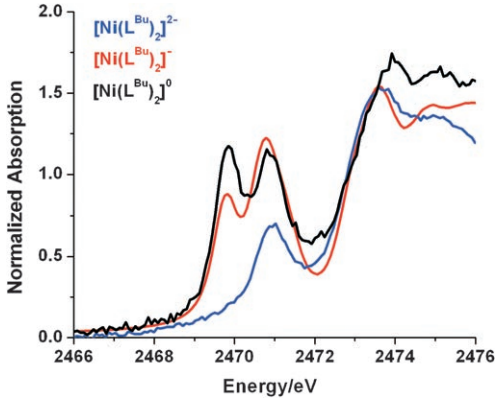

Figure 3. Comparison of the normalized S K-edge data for $[Ni(L^{Bu})_2]^0$, $[Ni(L^{Bu})_2]^-$, and $[Ni(L^{Bu})_2]^{2-}$.

$[Ni(L^{Bu})_2]^{2-}$, $[Ni(L^{Bu})_2]^{-}$, and $[Ni(L^{Bu})_2]^{0}$, showing very similar trends to those observed in reference [10]. All three complexes exhibit a pre-edge feature at ≈2471 eV, with similar intensity for the $[Ni(L^{Bu})_2]^{-}$ and $[Ni(L^{Bu})_2]^{0}$ complexes, and a decreased intensity for the dianionic complex (Table 1). In addition, the $[Ni(L^{Bu})_2]^{-}$ and $[Ni(L^{Bu})_2]^{0}$ both exhibit a lower energy pre-edge peak at ≈2470 eV, with an ≈30% increase in intensity (Table 1) observed upon oxidation of the $[Ni(L^{Bu})_2]^{-}$ complex to $[Ni(L^{Bu})_2]^{0}$. The rising edge position increases by ≈0.3 eV on going from the dianionic to the monoanionic to the neutral complex.

Ni monoanionic, dianionic, and neutral complexes—Ni K-edges: Figure 4 shows a comparison of the normalized Ni K-edge data for $[Ni(L^{Bu})_2]^{0}$, $[Ni(L^{Bu})_2]^{-}$, and $[Ni(L^{Bu})_2]^{2-}$. All three complexes have essentially identical pre-edge transition energies at ≈8332 eV (inset Figure 4). However, there are small changes in rising edge energies (8340–8350 eV) and more pronounced changes in the 8334–8340 eV "shakedown" region.

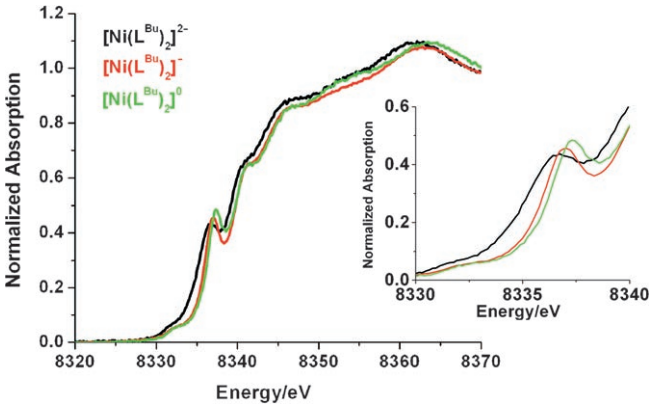

Figure 4. Comparison of the normalized Ni K-edge data for $[Ni(L^{Bu})_2]^{0}$, $[Ni(L^{Bu})_2]^{-}$, and $[Ni(L^{Bu})_2]^{2-}$. Inset shows an expansion of the pre-edge and shakedown region of the spectra.

Pt monoanionic and dianionic complexes—Pt L_3-edges: Figure S2 shows a comparison of the normalized Pt L_3-edges of the $[Pt(L^{Bu})_2]^{-}$ and $[Pt(L^{Bu})_2]^{2-}$ complexes. The virtually identical rising edge positions indicate that the effective charge on the metal has not changed.

Ni, Co, Cu monoanionic complexes—S K-edges: A comparison of the S K-edge data for $[Ni(L^{Bu})_2]^{-}$ complex (described above) to the $[Co(L^{Bu})_2]^{-}$ and $[Cu(L^{Bu})_2]^{-}$ complexes is shown in Figure 5. Fit parameters are summarized in Table 1. The S K-edge of $[Cu(L^{Bu})_2]^{-}$ has a single pre-edge peak at ≈2470.0 eV, with an integrated area of 1.52 units (Table 1). The $[Co(L^{Bu})_2]^{-}$ complex requires two features to fit the pre-edge at 2470.16 and 2470.77 eV (Table 1). The rising edge energy and shape for the $[Cu(L^{Bu})_2]^{-}$ and $[Co(L^{Bu})_2]^{-}$ complexes are very similar, while the rising edge of the Ni complex (at ≈2473.6 eV) decreases in intensity and shifts to slightly higher energy.

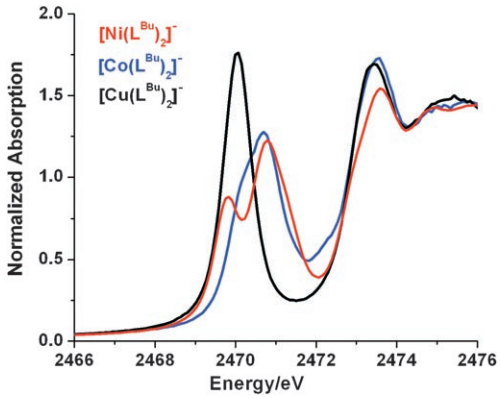

Figure 5. Comparison of the normalized S K-edge data for $[Cu(L^{Bu})_2]^{-}$, $[Ni(L^{Bu})_2]^{-}$, and $[Co(L^{Bu})_2]^{-}$.

Co, Cu monoanionic complexes—metal K- and L-edges: Figure 6 shows the normalized Cu L-edge data for $[Cu(L^{Bu})_2]^{-}$ as compared to that of D_{4h}-$[CuCl_4]^{2-}$. The L_3 and L_2 energies have increased by ≈2.5 eV relative to D_{4h}-$[CuCl_4]^{2-}$ and the intensity has decreased by ≈30%, consistent with the changes previously observed for Cu^{II}/Cu^{III} complexes.[31] Cu K-edge data were also obtained (Figure S3) and also show an increase (≈1 eV) in the pre-edge and rising edge energy relative to that of typical Cu^{II} complexes.

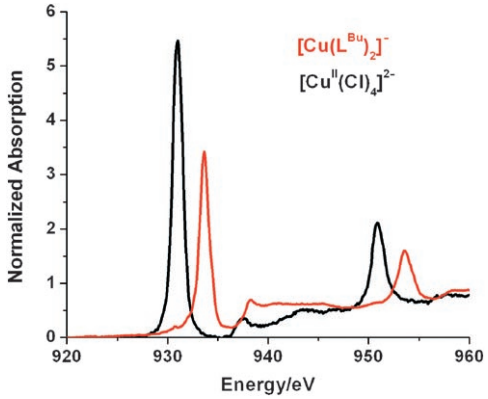

Figure 6. Normalized Cu L-edge data for $[Cu(L^{Bu})_2]^{-}$ compared to that of D_{4h}-$[CuCl_4]^{2-}$.

The Co L- and K-edge data for $[Co(L^{Bu})_2]^{-}$ were obtained and the spectra are provided in the Supporting Information (Figure S4). The Co K-edge data are similar in pre-edge and rising energy to that of known sulfur-ligated Co^{II} complexes, while the Co L-edge data appear intermediate between that of characterized Co^{II} and Co^{III} complexes.

Computational Results

All calculations have been performed for $[M(L)_2]^{z}$ complexes containing the unsubstituted benzene-1,2-dithiolato

L^{2-} ligand. The results are then compared with the experiments done on the corresponding $[M(L^{Bu})_2]^z$ complexes containing the 3,5-di-*tert*-butyl-benzene-1,2-dithiolato $L^{Bu\,2-}$ ligand.

Electronic structure: The electronic structures of the $[M(L)_2]^z$ complexes with M = Ni, Pd, Pt, Co and Cu for $z = -1$ and M = Au for $z = 0$ have been considered in detail before.[15b,17,10] It has been shown that the electronic spectra of such complexes can be well explained in terms of a simplified molecular orbital (MO) picture (Figure 7). While the

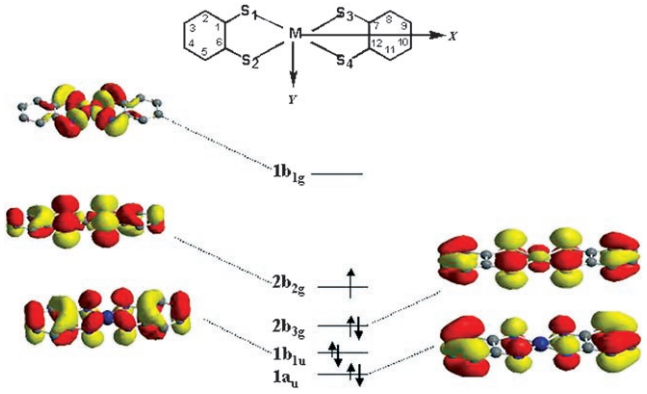

Figure 7. Simplified MO scheme for the $[M^{II}(L)(L^{\bullet})]^-$ (M = Ni, Pd, and Pt) and $[Au^{III}(L)(L^{\bullet})]$ complexes with a spin doublet ground state. For the $[Co(L)_2]^-$ complex the ground state is spin triplet with the $2b_{3g}$ and $2b_{2g}$ orbitals singly occupied. The corresponding $[M^{II}(L)_2]^{2-}$ (M = Ni, Pd, and Pt), and $[Cu^{III}(L)_2]^-$ complexes are diamagnetic with the $2b_{2g}$ orbital doubly occupied.

$1a_u$ and $1b_{1u}$ orbitals in Figure 7 represent pure ligand orbitals; the $2b_{2g}$, $2b_{3g}$ and the $1b_{1g}$ orbitals are shown to be delocalized over the metal and the ligand orbitals. The question of metal versus ligand oxidation in a series of transition-metal dithiolenes has thus been found to be dependent on the extent of delocalization in the redox active $2b_{2g}$ orbital, which is an antibonding combination between the ligand b_{2g} and the metal d_{xz} orbitals. Its character is mainly controlled by the effective nuclear charge of the central metal ion involved.

In the valence-isoelectronic $[M(L)_2]^-$ (M = Ni, Pd, Pt) and $[Au(L)_2]$ complexes, with the electron configuration $(1a_u)^2(1b_{1u})^2(2b_{3g})^2(2b_{2g})^1(1b_{1g})^0$, the b_{2g} orbital is predominantly ligand-based owing to the high effective nuclear charge of the metal. The electronic structures of these complexes[15b] have been described as being dominated by a closed-shell low-spin d^8 center metal bound to a delocalized class-III mixed valence radical anionic ligand as described by the resonance structures $[M^{II}(L)(L^{\bullet})]^- \leftrightarrow [M^{II}(L^{\bullet})(L)]^-$ (M = Ni, Pd, and Pt) and $[Au^{III}(L)(L^{\bullet})] \leftrightarrow [Au^{III}(L^{\bullet})(L)]$ ($L^{\bullet-}$ represents the one-electron oxidized radical anionic ligand). On the other hand, the electronic structures of the isoelectronic $[M(L)_2]^{2-}$ (M = Ni, Pd and Pt; L^{2-} represents the benzene dithiolato ligand) and $[Cu(L)_2]^-$ complexes with the electron configuration $(1a_u)^2(1b_{1u})^2(2b_{3g})^2(2b_{2g})^2(1b_{1g})^0$ are best described as $[M^{II}(L)_2]^{2-}$[15b] and $[Cu^{III}(L)_2]^-$,[15b,32] respectively. In all cases, the high-lying σ-antibonding metal d_{xy}-based MO $1b_{1g}$ is too high in energy to be able to accept an electron from the ligands. A subtle case was met in $[Co(L)_2]^-$ with the ground-state electronic configuration $(1a_u)^2(1b_{1u})^2(2b_{3g})^1(2b_{2g})^1(1b_{1g})^0$.[17a] In this case, the $2b_{2g}$ orbital possesses nearly equal metal and ligand characters and correspondingly, the electronic structure[17a] has been proposed to be best represented by the resonance forms $[Co^{III}(L)(L)] \leftrightarrow [Co^{II}(L^{\bullet})(L)] \leftrightarrow [Co^{II}(L)(L^{\bullet})]$.

Calculation of sulfur K-edge X-ray absorption spectra

Methodological aspects: It has been previously established that the analysis of the intensities of pre-edge transitions at the ligand K-edge provides a direct experimental method to address the covalencies of metal–ligand bonds.[18–20] In a recent study,[10] sulfur K-edge X-ray absorption spectroscopy (XAS) was used to probe the ground-state wavefunctions of the $[Ni(Me_2C_2S_2)_2]^{2-/-/0}$ complexes, which are directly relevant to the results of the present work. As discussed in detail earlier,[20] the oscillator strength of a given transition in the pre-edge region of the S (and Cl) XAS spectrum (apart from a proportionality constant) may be factored into two contributions: 1) the fractional sulfur (chlorine) character in the acceptor MO (α^2 referred to as "covalency") and 2) the radial transition-dipole integral $I(S) = |\langle S_{1s}|r|S_{3p}\rangle|^2$. Since $I(S)$ depends on several factors addressed below, it has been found necessary to determine its value for different types of bonding situations ($R-S^-$, R-S-S-R, S^{2-} etc) separately before values of α^2 can be determined from the areas under the experimental XAS absorption curves.

In the case of the $[Ni(Me_2C_2S_2)_2]^{2-/-/0}$ complexes, the transition dipole integral has been determined from the correlation of sulfur 1s→4p XAS edge energy positions of sulfide-, thiolate-, and enedithiolate. The M–L covalencies (α^2) were then determined on the basis of the relationship, $D_0 = (A/3n)\alpha^2 I(S)$, in which D_0 is the oscillator strength per sulfur atom, A is the ground state degeneracy, n is the number of S atoms contributing to the pre-edge feature ($n = 4$ in the present case).[10] For all the three oxidation states, the analysis revealed more than 50% sulfur character in the acceptor orbitals demonstrating the noninnocent behavior of the dithiolene ligand. The experimental covalencies were also correlated with DFT calculations to obtain further insight into geometric structure, spin distribution, spin polarization, and reactivity of the complexes.[10]

A critical point in the analysis is the value of the radial integral $I(S)$. Neither this value nor the value of α^2 is a physical observable. However, their product is directly related to the oscillator strength which *is* an observable. Since there always is an ambiguity in any factorization of an observable quantity, it is difficult to judge the accuracy of this methodology in the quantitative estimation of the metal–ligand covalencies. In this work, we have therefore chosen a different approach and *directly* calculated the physically observable quantity, for example, the oscillator strengths of the ob-

served transitions. We apply the factorization of $I(S)$ and α^2 *after* the correlation of the calculated and experimental oscillator strengths has been established. However, one still has to choose a reference complex for which the calculated metal–ligand mixing is accepted as reasonable before semi-empirical estimates of metal–ligand covalencies can be made for the remaining compounds. To this end we apply a rather simple but surprisingly successful TD-DFT based protocol that has been established from studying a series of simple metal–chloride complexes. Details of the calculations are described under "Computational methods".

Au Complexes—S K-edges: Figure 8 gives a comparison between the experimental and the TD-DFT-calculated S K-edge XAS spectra for the monoanionic and the neutral gold complexes. For the neutral $[Au(L^{Bu})_2]$ complex two pre-edge

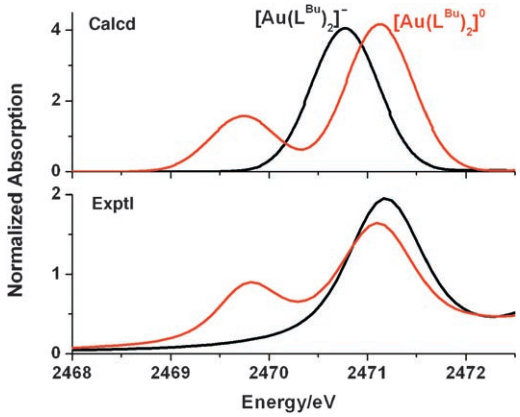

Figure 8. Experimental (bottom) and calculated (top) XAS spectra for the $[Au(L^{Bu})_2]^{-/0}$ complexes obtained from scalar relativistic ZORA-BP86 TDDFT calculations as described under "Computational methods".

transitions are calculated at energies of 2469.80 and 2471.17 eV, respectively, with an intensity ratio of 1.00:2.25. This is in excellent agreement with the experimentally observed transitions at 2469.80 and 2471.12 eV (intensity ratio 1.00:2.21). Owing to the agreement between the calculated and experimental results, the neutral $[Au(L^{Bu})_2]$ complex was further used as a reference for the conversion of experimentally determined peak areas to experimental oscillator strengths, which can then be directly compared with the calculated values. The results are summarized in Table 1 and show, with a few exceptions, very good agreement between the theoretical and experimental values. One of the less successful results has been met in the monoanionic $[Au(L^{Bu})_2]^-$ complex. In agreement with the experimental results, a single pre-edge transition is calculated. However, the calculations significantly underestimate the intensity of this transition, as is apparent from Figure 8.

Ni, Pd, Pt monoanionic complexes—S K-edges: Figure 9 represents the calculated XAS spectra for the $[M(L^{Bu})_2]^-$ (M = Ni, Pd, and Pt) complexes and their comparison with the ex-

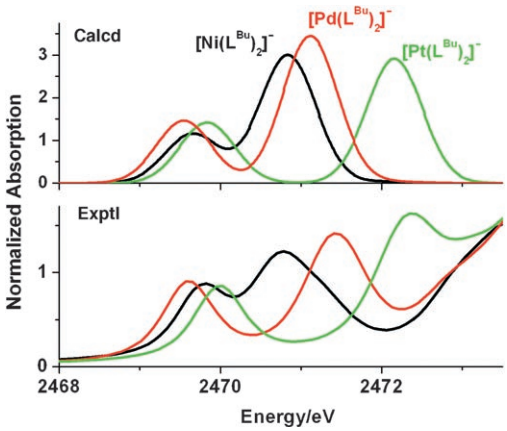

Figure 9. Experimental and calculated XAS spectra for the $[M(L^{Bu})_2]^-$ (M = Ni, Pd, and Pt) complexes obtained from scalar relativistic ZORA-BP86 TDDFT calculations as described under "Computational methods".

perimental spectra. Two pre-edge transitions are predicted for each of the complexes, in agreement with the experimental results. For all three complexes, the transition energies of the two pre-edge peaks, their splittings, and their intensities are very well reproduced in the calculations (compare Figure 9, and Table 1).

Co, Ni, Cu monoanionic complexes—S K-edges: As shown in Figure 10, the calculated pre-edge transitions for the $[M(L^{Bu})_2]^-$ (M = Co, Cu, and Ni) series are in reasonable agreement with the experimental results. For the $[Co(L^{Bu})_2]^-$ complex three pre-edge transitions are calculated at 2469.68 ($f_{osc} = 1.9 \times 10^{-4}$), 2470.06 ($f_{osc} = 4.1 \times 10^{-4}$), and 2471.30 eV ($f_{osc} = 11.5 \times 10^{-4}$), respectively. However, experimentally

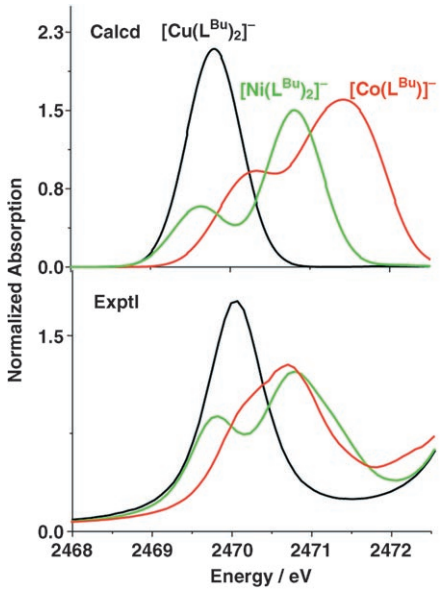

Figure 10. Experimental and calculated XAS spectra for the $[M(L)_2]^-$ (M = Co, Ni, and Cu) complexes obtained from scalar relativistic ZORA-BP86 TDDFT calculations.

only two pre-edge transitions are observed at 2470.16 ($f_{osc}=6.48\times10^{-4}$) and 2470.77 eV ($f_{osc}=11.90\times10^{-4}$). A plausible explanation is that the small splitting of ≈0.4 eV is simply not resolved in the experiments and hence a single peak at 2470.16 eV has been considered in the fitting. Note that the sum of the oscillator strengths for the first two calculated transitions (6.0×10^{-4}) is in good agreement with the experimental oscillator strength for the first pre-edge transition in $[Co(L^{Bu})_2]^-$ (6.48×10^{-4}). The third transition is calculated ≈0.6 eV too high in energy, which, based on the experience gained so far, is on the high side of the typical errors observed in the calculations. For the $[Cu(L^{Bu})_2]^-$complex, a single pre-edge transition is calculated at 2469.85 eV ($f_{osc}=17.0\times10^{-4}$), which is in good agreement with the experimentally observed transition at 2470.05 eV ($f_{osc}=15.59\times10^{-4}$).

Ni monoanioinic, dianionic, and neutral compolexes—S K-edges: The relative trends in energy and intensity for the $[Ni(L^{Bu})_2]^{2-/-}$ complexes are all well reproduced by TD-DFT calculations (Figure 11 and Table 1). The calculations have

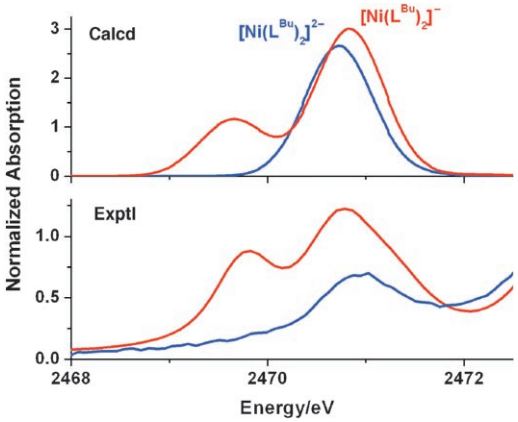

Figure 11. Experimental and calculated XAS spectra for the $[Ni(L^{Bu})_2]^{2-/-}$ complexes obtained from scalar relativistic ZORA-BP86 TDDFT calculations as described under "Computational methods".

not been extended to the neutral $[Ni(L^{Bu})_2]^0$. As explained previously,[15b] the ground state of this system features significant diradical character that cannot be adequately described in a single determinantal framework. Consequently, a linear-response treatment based on an inadequate ground state cannot be expected to yield reasonable results for excited states for which the intricate problems related to multideterminantal character are usually amplified in electronically excited states.

$[Ni(Me_2C_2S_2)_2]^{2-/-/0}$ S K-edges: Since the previous study on the $[Ni(Me_2C_2S_2)_2]^{2-/-/0}$ complexes[10] differed in significant details in the data analysis and interpretation to the present study, our calculations were extended to the $[Ni(Me_2C_2S_2)_2]^{2-/-/0}$ series. The calculated XAS spectra for the monoanionic $[Ni(Me_2C_2S_2)_2]^-$ and the dianionic $[Ni(Me_2C_2S_2)_2]^{2-}$ complexes are shown in Figure 12. For the

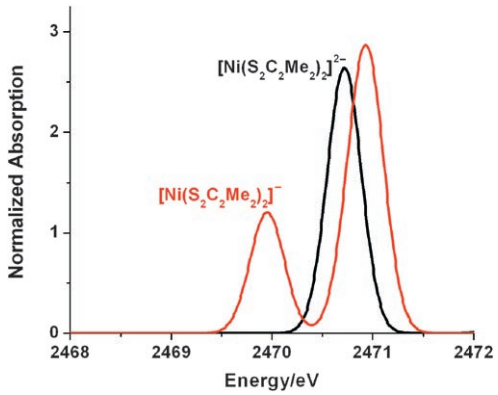

Figure 12. Calculated XAS spectra for the $[Ni(S_2C_2Me_2)_2]^{2-/-}$ complexes obtained from scalar relativistic ZORA-BP86 TDDFT calculations as described under "Computational methods".

monoanionic complex two pre-edge transitions are calculated at 2469.97 and 2470.98 eV, respectively, with an intensity ratio of 1:2.24. These transitions are experimentally observed at 2470.0 and 2471.0 eV, (intensity ratio 1:2.41), which must be considered as excellent agreement between theory and experiment. Interestingly, the SOMO to LUMO covalency ratio is calculated to be 1.23, which is in agreement with the results of the previous calculations. However, the covalency estimated from the pre-edge data of $[Ni(Me_2C_2S_2)_2]^-$ by using the Z_{eff} corrected transition dipole integral in reference [10] gave a reverse SOMO to LUMO covalency ratio (0.83) with respect to the calculations. This apparent discrepancy is resolved by the present calculations, which are in full agreement with experiment. The pre-edge transition for the dianionic $[Ni(Me_2C_2S_2)_2]^{2-}$ complex is calculated at a slightly lower energy and intensity relative to the values found by experiment, but the results are still reasonable. For the neutral complex no calculations were performed, owing to the limitations of the TD-DFT methodology in dealing with diradical systems alluded to above.

Discussion

Bonding description: Previously, it has been established that XAS spectra of transition-metal complexes with partly filled d-shells display intense pre-edge features in the region of the ligand K-edge that can be attributed to transitions from ligand 1s core electrons into delocalized MOs which are shared between the metal and the ligands.[18–20] In the recent work[10] these ideas were applied to the case of square-planar bis(dithiolene) ligands in order to obtain quantitative insights in their noninnocent nature. As developed earlier,[15b,17,10] and as evident from the bonding scheme shown in Figure 7, the $2b_{3g}$, $2b_{2g}$, and $1b_{1g}$ orbitals are important in the bonding description of these transition-metal complexes, since they represent the half-occupied or empty low-lying metal- and ligand-based MOs that can be probed by ligand K-edge XAS. Thus, in the pre-edge region of the S K-edge XAS spectra, transitions from the sulfur 1s levels to these

orbitals dominate the observed features. The $1b_{1g}$ orbital (antibonding combination of M $n\,d_{xy}$ and the bis(dithiolene) b_{1g} orbitals) provides an efficient pathway for the ligand-to-metal σ donation, whereas the $2b_{3g}$ (antibonding combination of the M $3d_{yz}$ and the bis(dithiolene) b_{3g} orbitals) and $2b_{2g}$ (antibonding combination of the M $3d_{xz}$ and the bis(dithiolene) b_{2g} orbitals) orbitals account for the metal-to-ligand π-electron back-donation. This super-exchange pathway has been found to be dominant for the highly efficient antiferromagnetic coupling in the neutral, diradical bis(*o*-diiminobenzosemiquinonato) (L^N) transition-metal complexes $[M^{II}(L^{N\bullet})(L^{N\bullet})]$ (M = Ni, Pd, Pt),[33] which have closely analogous electronic structures to the analogous bis(dithiolene) complexes studied here. The diamagnetic $[M(L)_2]^z$ (M = Ni, Pd, Pt for $z=2-$; M = Cu, Au for $z=1-$) complexes possess the ground state electronic configuration $(1a_u)^2(1b_{1u})^2(2b_{3g})^2(2b_{2g})^2(1b_{1g})^0$. A single pre-edge transition is observed in the XAS spectra,[10] which is assigned to a sulfur 1s to $1b_{1g}$ transition (referred to as a "σ transition") on the basis of the TD-DFT calculations. In contrast, two pre-edge transitions are observed in the XAS spectra of the spin doublet $[M(L)(L^{\bullet})]^z$ (M = Ni, Pd, Pt for $z=-1$; M = Au for $z=0$) complexes with the ground-state electronic configuration $(1a_u)^2(1b_{1u})^2(2b_{3g})^2(2b_{2g})^1(1b_{1g})^0$. The higher energy feature again corresponds to the sulfur 1s to $1b_{1g}$ transition. The appearance of a second lower energy pre-edge feature in the $[M(L)(L^{\bullet})]^z$ complexes is attributed to a sulfur 1s to $2b_{2g}$ transition (referred to as a "π transition").[10] The corresponding $[Co(L)_2]^-$ complex possesses a spin triplet ground state with an electronic configuration of $(1a_u)^2(1b_{1u})^2(2b_{3g})^1(2b_{2g})^1(1b_{1g})^0$. Due to the presence of an additional (S3p) hole in the $2b_{3g}$ orbital, the three pre-edge transitions (two π and one σ) can only be resolved experimentally as two peaks—a low-energy peak corresponding to the two π transitions and a higher energy peak corresponding to the σ transition.

Figure 13 establishes the correlation between the experimental and the calculated results for the complexes. A linear dependence between the experimental peak area and the calculated oscillator strength is observed for all complexes except the monoanionic $[Au(L)_2]^-$ and dianionic $[Ni(L)_2]^{2-}$ complexes, for which the dipolar intensities have been largely underestimated and overestimated, respectively, in the calculations. Moreover, the calculated oscillator strengths for the $2b_{3g}$, $2b_{2g}$ and $1b_{1g}$ transitions show an almost exact linear dependence on the amount of S3p character (based on a Löwdin partitioning analysis) in the partially occupied acceptor MOs in all of the $[M(L)_2]^z$ complexes (Figure 14), in agreement with the results of previous experimental and theoretical studies.[18–20] The slope of this plot will then yield the transition dipole integral, $I(S)$, for the benzenedithiol ligand. It is most interesting to observe, that the present study reveals that the dipole integrals obtained in this way are *lower* for the π transitions than for the σ transitions, as reflected by the 20% decrease in the slope. The dependence of $I(S)$ on the acceptor orbital is particularly important for quantitative measures of S3p character in highly covalent complexes. This is a new result, since in previous studies, the transition dipole integral has been assumed to depend only of the effective charge on the sulfur and to be independent of the acceptor orbital.

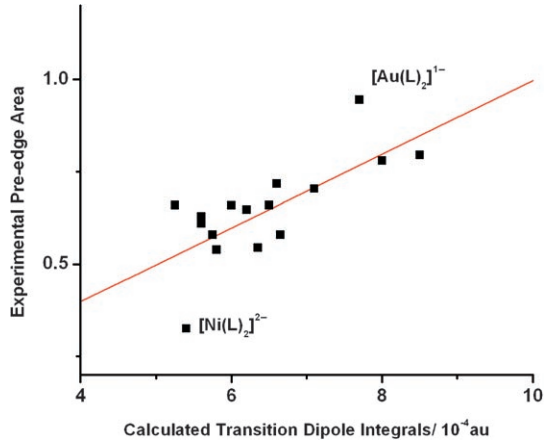

Figure 13. Experimental pre-edge area versus ZORA BP86 TDDFT calculated dipole contribution plot for the complexes.

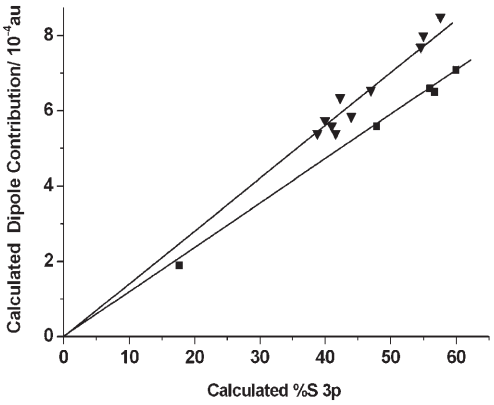

Figure 14. ZORA BP86 TDDFT calculated dipole contribution versus percentage S3p character per hole plot for σ (▼; slope = 0.144) and π transitions (■; slope = 0.120) in $[M(L^{Bu})_2]^z$ complexes.

Our rationale for the observed dependence is analogous to the previous analysis of anisotropic "central-field" covalency in transition-metal complexes: based on the fundamental results of Rüdenberg and co-workers,[34] atomic orbitals in bonding MOs tend to contract, while those in antibonding orbitals tend to expand in order to maintain the energetic balance required by the virial theorem. The degree of radial distortion depends on the amount of overlap between the constituent atomic or fragment orbitals. Therefore, it is not entirely surprising, that π and σ bonds differ in their degree of radial distortion and this is naturally reflected by the calculated oscillator strengths. The present analysis indicated that the orbitals involved in the π transitions are more contracted than those involved in the σ transitions, which is consistent with the fact that these orbitals are less strongly antibonding than their σ counterparts involved in

the $1b_{1g}$ MO. Consequently, the value of $I(S)$ is considerably smaller for a π relative to a σ transition.

These results indicate that different standards are necessary for σ and π pre-edge transitions in order to accurately quantify the covalency of the valence orbitals of the $[M(L)_2]^z$ complexes; this fact is of particular importance for highly covalent complexes, in which the difference in the radial distortion of π versus σ bonds will be most pronounced. Once more, the neutral $[Au(L)_2]$ complex will be used for this purpose, since the calculations accurately reflect the trends in transition energy and intensity in this case. Based on this reasoning, 1.56 units of σ pre-edge intensity correspond to 110% sulfur 3p character over the two $1b_{1g}$ holes (e.g. 55% sulfur character in the $1b_{1g}$ orbital). Likewise, 0.704 units of π pre-edge intensity correspond to 60% sulfur 3p character in the $2b_{2g}$ (or $2b_{3g}$) hole. Based on these values a semiempirical estimate of metal–ligand covalencies is obtained for the remaining complexes in the $[M(L)_2]^z$ series. The results are summarized in Table 2.

Table 2. Calculated and experimental covalencies for the complexes.

	Transitions	Experimental covalency[a]	Calculated covalency
$[Ni(L)_2]^-$	$S\rightarrow 2b_{2g}$	53.6	47.9
	$S\rightarrow 1b_{1g}$	76.8	84.6
$[Pd(L)_2]^-$	$S\rightarrow 2b_{2g}$	61.1	56.0
	$S\rightarrow 1b_{1g}$	81.8	94.0
$[Pt(L)_2]^-$	$S\rightarrow 2b_{2g}$	56.2	56.7
	$S\rightarrow 1b_{1g}$	86.0	82.0
$[Au(L)_2]^0$	$S\rightarrow 2b_{2g}$	60.0	60.0
	$S\rightarrow 1b_{1g}$	110.0	110.0
$[Au(L)_2]^-$	$S\rightarrow 1b_{1g}$	133.2	109.2
$[Cu(L)_2]^-$	$S\rightarrow 1b_{1g}$	107.1	115.2
$[Ni(L)_2]^{2-}$	$S\rightarrow 1b_{1g}$	45.9	77.6
$[Ni(L)_2]$	$S\rightarrow 2b_{2g}$	76.7	[b]
	$S\rightarrow 1b_{1g}$	74.0	
$[Pd(L)_2]^{2-}$	$S\rightarrow 1b_{1g}$	[c]	88.2
$[Pt(L)_2]^{2-}$	$S\rightarrow 1b_{1g}$	[c]	83.1
$[Co(L)_2]^-$	$S\rightarrow 2b_{3g}$	56.1	52.5
	$S\rightarrow 2b_{2g}$		
	$S\rightarrow 1b_{1g}$	81.8	80.0
$[Ni(S_2C_2Me_2)_2]^-$	$S\rightarrow 2b_{2g}$	46.2	51.2
	$S\rightarrow 1b_{1g}$	91.2	83.4
$[Ni(S_2C_2Me_2)_2]^{2-}$	$S\rightarrow 1b_{1g}$	93.0	76.8

[a] Neutral $[Au(L^{Bu})_2]^0$ calibrated experimental covalency. [b] Calculations were not performed. [c] Feature is not well-resolved from edge and therefore accurate areas (covalencies) cannot be obtained.

Au complexes: The pre-edge intensity of the monoanionic $[Au(L^{Bu})_2]^-$ complex corresponds to 133% of S3p character (α^2). In the calculation, however, the S3p character (109%) of the $1b_{1g}$ level is underestimated. For the neutral $[Au(L^{Bu})_2]$ form, the pre-edge intensity of the high- and low-energy pre-edge features give 110 and 60% of S3p character, respectively. The total ligand character is, in fact, larger due to the non-negligible contributions from the C and H atoms in the aromatic ring. (10–30%; Table S1). The oxidation of $[Au(L^{Bu})_2]^-$, thus, creates an additional hole in the $2b_{2g}$ level with more than 50% of S3p character. This means that, upon oxidation of the monoanionic form, more than 50% of the electron density is lost from a sulfur-based orbital, which is consistent with a predominantly ligand based oxidation of the $[Au(L^{Bu})_2]^{-/0}$ couple. This is in agreement with the results of the previous EPR, ^{197}Au Mössbauer, and DFT studies on the $[Au(L^{Bu})_2]^{-/0}$ complexes.[15b,17c] The ligand-based oxidation is further supported by the ≈0.25 eV increase in the S K-rising-edge inflection point on going from the monoanionic (2473.0 eV) to the neutral (2473.25 eV) complex, and also from the identical Au L_3-rising-edge inflection points in $[Au(L^{Bu})_2]^-$ and $[Au(L^{Bu})_2]$.

Ni, Pd, Pt monoanionic complexes: The $[M(L)_2]^-$ (M = Ni, Pd, Pt) complexes possess a common ground state $^2B_{2g}$, with an electronic configuration of $(1a_u)^2(1b_{1u})^2(2b_{3g})^2(2b_{2g})^1(1b_{1g})^0$. All three complexes show two pre-edge features; a lower energy feature corresponding to a sulfur 1s to $2b_{2g}$ transition and a higher energy feature assigned to a sulfur 1s to $1b_{1g}$ transition. The calibrated experimental covalencies yield more than 50% of S3p character in the singly occupied molecular orbital ($2b_{2g}$, SOMO) for each of the Ni, Pd, and Pt monoanions (Table 2). Thus the SOMO is predominantly ligand-based, which is consistent with the findings of our previous studies on the $[M(L^{Bu})_2]^-$ complexes, in which their electronic structure has been described in terms of an M^{II} d^8 ion bound to both the dithiolato(2−) and the dithiobenzosemiquinonato(−) forms of the ligand.[15b,17] The lowest unoccupied molecular orbital ($1b_{1g}$, LUMO) is, however, predominantly metal-based in the whole series (Table 2). The energy of the lower energy pre-edge transition to the $2b_{2g}$ level is therefore independent on the central metal ion, and does not change significantly (Figure 9) across the $[M(L^{Bu})_2]^-$ series. The pre-edge transition to the $1b_{1g}$ orbital, on the other hand, shows dramatic changes (Figure 9) in energy as the effective nuclear charge of the central metal ion is increased. Consequently, this higher energy S K-edge XAS feature in the series directly provides insight into the strength of the metal–ligand σ bonds. The bond strengths increase with increasing transition energy, which reflects the increasing destabilization of the $1b_{1g}$ orbital through increased metal–ligand interactions.

Experimentally, a decrease in the SOMO covalency in the order $[Pd(L)_2]^- > [Pt(L)_2]^- > [Ni(L)_2]^-$ is observed (and a similar trend is observed for the dianionic complexes across this series, Figure S1). This trend is also nicely reproduced in the calculations (Table 2). This supports the "inverted-bonding scheme" for the complexes, in which the ligand orbitals are situated higher in energy than the metal d orbitals, as has been suggested previously by Szilagyi et al. for similar complexes.[10] In the present study, this dependence is formulated in terms of increasing radical character of the bis(dithiolene) ligand which, as described in reference [15b], exist in a delocalized class III mixed valence situation in these monoanions.

Ni monoanioinc, dianionic, and neutral complexes: The intensity of the only observed pre-edge peak in the dianionic

$[Ni(L^{Bu})_2]^{2-}$ complex corresponds to 46% $S3p_\sigma$ character, while, for the monoanionic form, the high- and low-energy pre-edge features give 77% $S3p_\sigma$ and 54% $S3p_\pi$ character, respectively. Finally, the intensities of the high- and low-energy features in the neutral $[Ni(L^{Bu})_2]$ complex correspond to covalencies of 74% $S3p_\sigma$ and 77% $S3p_\pi$ character, respectively. Based on the MO picture shown in Figure 7, the calculated covalency of the $1b_{1g}$ orbital increases on going from the dianionic to the monoanionic complex, in good agreement with the pre-edge data. On a quantitative level (Table 2), the calculations on the $[Ni(L^{Bu})_2]^{2-}$ dianion significantly overestimate the ligand character in the $1b_{1g}$ orbital (78%) compared to the experimental estimate (46%). The calculated covalencies (85, 48%) for the monoanionic complex are, however, in quite good agreement with the experimental values (77, 54%). In any case, the frontier orbitals of the $[Ni(L^{Bu})_2]^{2-/-/0}$ complexes have mainly S-ligand character, which is in agreement with the results of the study by Szilagyi et al.[10] The 0.3 eV shift of the edge positions to higher energy in going from the dianionic to the monoanionic and to the neutral complex further supports the ligand based redox processes in the $[Ni(L^{Bu})_2]^{2-/-/0}$ series.

To confirm this conclusion from the perspective of the central metal atom, an additional set of XAS data was measured at the Ni K-edge. The spectra of the $[Ni(L^{Bu})_2]^{2-/-/0}$ complexes possess essentially identical pre-edge transition energies ($\approx$8332 eV, inset in Figure 4), indicating that the effective nuclear charge on the metal is similar in all the three complexes. Comparison to known Ni^{II} complexes[35] shows all three edges to be slightly more oxidized than typical Ni^{II} complexes with similar ligation. For the $[Ni(L^{Bu})_2]^-$ and $[Ni(L^{Bu})_2]^0$ complexes, the rising edge regions (8340–8350 eV) are essentially identical, further supporting a similar oxidation state on the metal in both complexes. However, for the $[Ni(L^{Bu})_2]^{2-}$ complex, the rising edge has shifted down by $\approx$0.4 eV, indicating that the metal in this complex may be more reduced than that of the monoanionic and neutral complexes. In addition, there are pronounced changes in the spectra in the 8334–8340 eV region. The shoulder that appears in this region is assigned as a 1s-to-4p and ligand-to-metal charge-transfer (LMCT) shakedown transition. This is formally a two-electron transition, which occurs due to the relaxation of primarily metal-based levels below that of the primarily ligand-based levels due to the formation of a Ni 1s core hole. This feature increases by $\approx$1.0 eV on going from the dianionic to monoanionic to the neutral complex. Even if one accounts for the 0.4 eV shift observed in the rising edge of the $[Ni(L^{Bu})_2]^{2-}$ complex, there is still a $\approx$0.6 eV change that is not accounted for and this may be attributed to changes at the ligand. In particular, the increase in the shakedown transition energy on going from $[Ni(L^{Bu})_2]^{2-}$ to $[Ni(L^{Bu})_2]^-$ to $[Ni(L^{Bu})_2]^0$ is consistent with increasing ligand oxidation, which would lower the ligand 3p orbitals and result in a shakedown feature at higher energy. This trend further supports the primarily ligand-based redox processes in this series of nickel complexes.

Co, Ni, Cu monoanionic complexes: Three pre-edge transitions are calculated for the $[Co(L^{Bu})_2]^-$ complex corresponding to sulfur 1s to $2b_{3g}$, $2b_{2g}$, and $1b_{1g}$ transitions (Table 1). The first two transitions occur at similar energies and are not resolved in the experimental spectra. The calculated combined $S3p_\pi$ character of the $2b_{2g}$ and $2b_{3g}$ orbitals in $[Co(L^{Bu})_2]^-$ is 53% (18% for $2b_{3g}$ and 35% for $2b_{2g}$), which is in good agreement with the experimentally estimated covalency of 56% from the intensity of the low-energy pre-edge feature in $[Co(L^{Bu})_2]^-$. The higher energy pre-edge intensity leads to an estimate of 82% of LUMO ($1b_{1g}$) σ covalency compared to 80% obtained in the calculation. It is interesting to compare this data to the results obtained for $[Ni(L^{Bu})_2]^-$. In this case, the experimental covalencies of the $2b_{2g}$ and $1b_{1g}$ orbitals have been estimated to be 54 and 77%, respectively (vide supra). Thus, experimentally a considerable increase in the π covalency is observed upon going from the $[Co(L^{Bu})_2]^-$ complex (56% of $S3p_\pi$ character over two holes) to the $[Ni(L^{Bu})_2]^-$ complex (54% of $S3p_\pi$ character over a single $2b_{2g}$ hole). This result confirms the notion that the radical character in the Ni series is considerably higher than in the case of a central cobalt ion and is also nicely reproduced in the calculations (Table 2). A S3p character of 107% over the two $1b_{1g}$ holes has been estimated for the corresponding $[Cu(L^{Bu})_2]^-$ complex in reasonable agreement with the calculated covalency of 115%. It is of interest to note that the rising-edge energy and shape for the $[Cu(L^{Bu})_2]^-$ and $[Co(L^{Bu})_2]^-$ complexes are very similar, while the sulfur 1s→C–S σ* transition of the Ni complex (at $\approx$2473.6 eV) decreases in intensity and shifts to slightly higher energy. This indicates that the ligand in $[Ni(L^{Bu})_2]^-$ is more oxidized than that of the corresponding cobalt and copper complexes. All of these results are in agreement with the earlier conclusions[15b,17a] that the monoanionic copper complex features an essentially innocent ligand, while the case of cobalt is ambiguous.

To further corroborate this assignment, an additional set of XAS data was obtained at the Cu L-edge. The XAS spectrum of $[Cu(L^{Bu})_2]^-$ shows an increase in the Cu $L_{3,2}$-edge energies by $\approx$2.5 eV relative to that of $[CuCl_4]^{2-}$ (Figure 6), thus supporting the previous Cu^{III} oxidation state assignment for this compound. It is of interest to note that the L_3 and L_2 intensities decrease dramatically in the $[Cu(L^{Bu})_2]^-$ complex relative to $[CuCl_4]^{2-}$. This decrease in intensity, despite the formation of an additional d-hole, reflects the highly covalent nature of the $[Cu(L^{Bu})_2]^-$ complex, which must be expected for the oxidation state Cu^{III} ligated by thiolate sulfur atoms. Indeed, the highly covalent nature of the Cu^{II}–S_{cys} bond has been extensively discussed for the blue copper proteins.[36a–e] as well as for Cu_A centers.[21b,36e–g] Finally, Co K- and L-edge data of the $[Co(L^{Bu})_2]^-$ complex have been obtained. On a phenomenological level, they lead to conflicting assignments of the oxidation state of the central Co ion. The K-edge data support a Co^{II} assignment, while the latter appear intermediate between Co^{II} and Co^{III}; however, without a full multiplet analysis, which is beyond the scope of the present work, a definitive assignment cannot be made

and we take these results, together with the extensive set of theoretical and experimental data obtained previously,[17a] as an additional indication that the oxidation state of Co is ambiguous in $[Co(L^{Bu})_2]^-$.

Conclusions

The most important goal of the present investigation is the experimental quantitation of ground-state covalencies in a series of square-planar bis(3,5-di-*tert*-butyl-benzene-1,2-dithiolato) transition-metal complexes, based on S K-edge XAS pre-edge intensities. The analysis together with the considerable body of previous work[9b,10,15b,17] reveals that the question of metal versus ligand oxidation in such complexes can be addressed by comparing the covalency of the redox-active $2b_{2g}$ orbital (an antibonding combination of the metal d_{xz} and out-of-plane ligand-π orbitals with significant sulfur contribution). The present work complements previous structural, electrochemical, EPR, absorption, MCD and resonance Raman investigations.[15b,17] Here, quantitative estimates of the open-shell character of the dithiolate ligands have been achieved though XAS spectroscopy at the ligand K-edge together with complementary measurements at the metal K- and L-edges. The data were analyzed by direct TD-DFT-based calculations of the XAS spectra. The calculated transition energies and intensities are, with a few exceptions, in very good agreement with the experimental values. Semiempirical estimates of the metal–ligand covalencies are then made considering the neutral $[Au(L^{Bu})_2]$ complex as a reference, for which the calculated metal–ligand mixing is considered to be reasonable. Thus, the present study deviates in an important methodological aspect from previous interpretations of S K-edge data.[10,21] All previous studies are based on the factorization of the oscillator strengths into a factor coming from the metal–ligand mixing (α^2) and a radial transition dipole integral I(S). These studies have obtained a value of I(S) experimentally (using other spectroscopic methods) for a given type of sulfur (thiolate, sulfide, dithiolene, etc.) and extrapolated this to the metal–ligand complex based on shifts in the rising-edge energies. In the present work, we have used the fact that neither I(S) nor α^2 represent physical observables, but that their product is proportional to the oscillator strength which *is* an observable. Consequently, we have applied the factorization *a posteri* after the calculation of the oscillator strengths.[10,21] In taking this approach, it was found that for the present series of molecules, it is necessary to introduce two distinct values for I(S)—one for 1s→σ ($1b_{1g}$ acceptor MO) transitions and one for 1s→π ($2b_{2g}$ or $2b_{3g}$ acceptor MOs) transitions. The change in I(S) has been plausibly attributed to the different degrees of radial distortion of the sulfur 3p orbitals, which is particularly important in highly covalent σ and π bonds.

Based on the combined experimental and theoretical estimates, insight into the noninnocent nature of the dithiolate ligand in the series of $[M(L^{Bu})_2]^{n-}$ complexes has been obtained. The results of the semiempirical estimates show more than 50% S3p character for the $2b_{2g}$ SOMO of the monoanions of Ni, Pd, and Pt as well as the neutral Au complex. Thus these complexes are best viewed as delocalized class III mixed-valence ligand radicals coordinated to a closed-shell low-spin d^8 central metal; the radical character (or the percentage S3p character in the $2b_{2g}$ SOMO), however, decreases in the order $[Au(L^{Bu})_2] \approx [Pd(L^{Bu})_2]^- > [Pt(L^{Bu})_2]^- > [Ni(L^{Bu})_2]^-$. This is attributed to the variation in the d orbital energies relative to the ligand, which in turn is dependent on the Z_{eff} and the relativistic potential that mainly influences the energetic position of the d-shell at the central metal ion. The situation may be explained in a simple way by reference to Figure 15, in which the calculated energy of the metal d_{xz} orbital relative to the ligand π*-b_{2g} orbital energy is plotted for the different complexes in the $[M(L^{Bu})_2]^z$ series. Due to the high effective nuclear charge of the Pd^{II} and Au^{III} ions, the metal d_{xz} orbitals in $[Pd(L^{Bu})_2]^-$ and $[Au(L^{Bu})_2]$ are situated at very low energy so that the metal–ligand mixing is minimal, providing maximum ligand character (≈60% S3p character in the SOMO) to the complexes. In the corresponding $[Co(L^{Bu})_2]^-$ complex, however, the Co d_{xz} orbital is situated at a comparable energy to the ligand orbital providing considerable metal–ligand mixing in the $2b_{2g}$ SOMO (45% S3p character). Thus, as deduced from extensive previous studies,[17a] an ambiguous case is met in $[Co(L^{Bu})_2]^-$ in which the oxidation state of the central cobalt cannot be unambiguously assigned. For all metals before Co in the first-row transition-metal series, the metal d_{xz} orbital is predicted to be at a higher energy than the ligand orbital. Metal-based redox processes are thus expected for their bis(dithiolene) complexes. This has been found to be the case in the previous studies on the $[Fe(L^{Bu})_2]^{2-}$[17a] and $[CrO(L^{Bu})_2]^-$[37] complexes. The only reason that the redox chemistry does not occur in the case of $[Cu(L^{Bu})_2]^-$ is the electron count—the acceptor d_{xz} orbital is filled in the case of a Cu^{III} with a d^8 configuration and the only possible acceptor orbital at the copper atom, the d_{xy} based b_{1g} orbital, is energetically inaccessible. Thus, despite the high effective nuclear charge of the central Cu^{III} oxidation of the ligand does not occur.

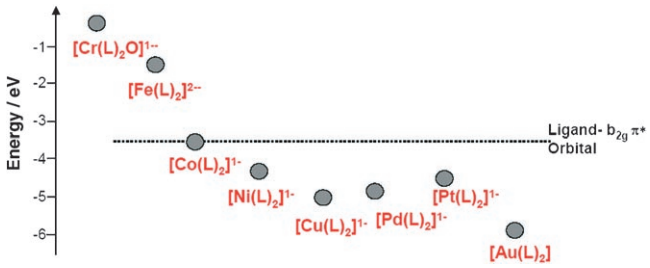

Figure 15. Calculated energy of the metal d_{xz} orbital relative to the ligand π*-b_{2g} orbital energy for the different complexes in the $[M(L)_2]^{n-}$ series.

Taken together, we believe the present study provides detailed insight into the covalencies and bonding descriptions

of transition-metal dithiolenes. We hope that these insights will prove useful in further characterizing the biological Mo– and W–dithiolenes and biologically relevant model complexes, and therefore help to address the questions of whether the dithiolene ligand, in such compounds, could possibly act as a noninnocent ligand, which would certainly have significant implications for the reactivity of such sites.

Acknowledgements

We are grateful to the Fonds der Chemischen Industrie and the NSF (CHE-0446304 to E.I.S.) for financial support. SSRL operations are funded by the Department of Energy, Office of Basic Energy Sciences. The Structural Molecular Biology program is supported by the National Institutes of Health, National Center for Research Resources, Biomedical Technology Program and by the Department of Energy, Office of Biological and Environmental Research. K.R. thanks the Max-Planck Society for a stipend.

[1] a) C. Enroth, B. T. Eger, K. Okamoto, T. Nishino, T. Nishino, E. F. Pai, *Proc. Natl. Acad. Sci. USA* **2000**, *97*, 1599; b) R. C. Bray, B. G. Malmström, T. Vänngard, *Biochem. J.* **1959**, *73*, 193; c) R. Hille, T. Nishino, *FASEB J.* **1995**, *9*, 995; d) R. Hille, *Chem. Rev.* **1996**, *96*, 2757; e) W. Campbell, *Plant Physiol.* **1996**, *111*, 355; f) L. P. Solomonson, M. P. Barber, *Plant Mol. Biol.* **1990**, *41*, 225; g) H. -L. Li, C. Temple, K. V. Rajagopalan, H. Schindfelin, *J. Am. Chem. Soc.* **2000**, *122*, 7673; h) R. Cammack, J. H. Weiner, *Biochemistry* **1990**, *29*, 8410; i) P. Ellis, T. Conrads, R. Hille, P. Kuhn, *Structure* **2001**, *9*, 125; j) G. L. Anderson, J. Williams, R. Hille, *J. Biol. Chem.* **1992**, *267*, 23674; k) S. Mukund, M. W. W. Adams, *J. Biol. Chem.* **1991**, *266*, 14208.

[2] a) B. S. Lim, K. M. Sung, R. H. Holm, *J. Am. Chem. Soc.* **2000**, *122*, 7410; b) B. S. Lim, R. H. Holm, *J. Am. Chem. Soc.* **2001**, *123*, 1920; c) B. S. Lim, J. P. Donahue, R. H. Holm, *Inorg. Chem.* **2000**, *39*, 263; d) K. M. Sung, R. H. Holm, *Inorg. Chem.* **2001**, *40*, 4518; e) K. M. Sung, R. H. Holm, *J. Am. Chem. Soc.* **2001**, *123*, 1931.

[3] a) G. N. Schrauzer, *Transition Met. Chem.* **1968**, *4*, 299; b) J. A. McCleverty, *Prog. Inorg. Chem.* **1968**, *10*, 49; c) R. H. Holm, M. J. O'Connor, *Prog. Inorg. Chem.* **1971**, *14*, 241; d) R. Eisenberg, *Prog. Inorg. Chem.* **1970**, *12*, 295; e) H. B. Gray, *Transition Met. Chem.* **1965**, *1*, 240; f) "Dithiolene Chemistry: Synthsis, Properties, and Applications": *Progr. Inorg. Chem.* **2004**, *52*, whole volume.

[4] a) D. Sellmann, H. Binder, D. Häussinger, F. W. Heinemann, J. Sutter, *Inorg. Chim. Acta* **2000**, *300–302*, 829; b) K. Mrkvova, J. Kameni, Z. Sindela, L. Kvitek, *Transition Met. Chem.* **2004**, *29*, 238.

[5] D. T. Sawyer, G. S. Srivatsa, M. E. Bodini, W. P. Schaefer, R. M. Wing, *J. Am. Chem. Soc.* **1986**, *108*, 936.

[6] a) D. Sellmann, G. Freyberger, R. Eberlein, E. Böhlen, G. Huttner, L. Zsolnai, *J. Organomet. Chem.* **1987**, *323*, 21; b) D. Sellmann, O. Käppler, *Z. Naturforsch. B* **1987**, *42*, 1291.

[7] E. I. Stiefel, J. H. Waters, E. Billig, H. B. Gray, *J. Am. Chem. Soc.* **1965**, *87*, 3016.

[8] a) A. L. Balch, R. H. Holm, *J. Am. Chem. Soc.* **1966**, *88*, 5201; b) R. H. Holm, M. J. Olanov *Prog. Inorg. Chem.* **1971**, *14*, 241.

[9] a) B. S. Lim, D. V. Fomitchev, R. H. Holm, *Inorg. Chem.* **2001**, *40*, 4257; b) V. Bachler, G. Olbrich, F. Neese, K. Wieghardt, *Inorg. Chem.* **2002**, *41*, 4179.

[10] R. K. Szilagyi, B. S. Lim, T. Glaser, R. H. Holm, B. Hedman, K. O. Hodgson, E. I. Solomon, *J. Am. Chem. Soc.* **2003**, *125*, 9158.

[11] D. Sellmann, M. Geck, F. Knoch, G. Ritter, J. Denglar, *J. Am. Chem. Soc.* **1991**, *113*, 3819.

[12] H. Alves, D. Simao, H. Novais, I. C. Santos, C. Gimenez-Saiz, V. Gama, J. C. Waerenborgh, R. T. Henriques, M. Almeida, *Polyhedron* **2003**, *22*, 2481.

[13] C. G. Pierpont, C. W. Lange, *Prog. Inorg. Chem.* **1994**, *41*, 331.

[14] a) Y. Qin, R. A. Wheeler, *J. Am. Chem. Soc.* **1995**, *117*, 6083; b) F. Himo, A. Gräslund, L. A. Erikson, *Biophys. J.* **1997**, *72*, 1556; c) R. Adamo, A. Subra, A. Di Matteo, V. Barone, *J. Chem. Phys.* **1998**, *109*, 10244.

[15] a) G. N. R. Tripathi, Q. Sun, D. A. Armstrong, D. M. Chipman, R. H. Schuler, *J. Phys. Chem.* **1992**, *96*, 5344; b) K. Ray, T. Weyhermüller, F. Neese, K. Wieghardt, *Inorg. Chem.* **2005**, *44*, 5345.

[16] K. Wang, E. I. Stiefel, *Science* **2001**, *291*, 106.

[17] a) K. Ray, A. Begum, T. Weyhermüller, S. Piligkos, F. Neese, K. Wieghardt, *J. Am. Chem. Soc.* **2005**, *127*, 4403; b) K. Ray, E. Bill, T. Weyhermüller, K. Wieghardt, *J. Am. Chem. Soc.* **2005**, *127*, 5641; c) K. Ray, T. Weyhermüller, A. Goossens, M. W. J. Crajé, K. Wieghardt, *Inorg. Chem.* **2003**, *42*, 4082; d) T. Petrenko, K. Ray, K. Wieghardt, F. Neese, *J. Am. Chem. Soc.* **2006**, *128*, 4422.

[18] a) E. I. Solomon, B. Hedman, K. O. Hodgson, A. Dey, R. K. Szilagyi, *Coord. Chem. Rev.* **2005**, *249*, 97; b) S. E. Shadle, J. E. Penner-Hahn, H. J. Schugar, B. Hedman, K. O. Hodgson, E. I. Solomon, *J. Am. Chem. Soc.* **1993**, *115*, 767.

[19] T. Glaser B. Hedman, K. O. Hodgson, E. I. Solomon, *Acc. Chem. Res.* **2000**, *33*, 859.

[20] a) F. Neese, B. Hedman, K. O. Hodgson, E. I. Solomon, *Inorg. Chem.* **1999**, *38*, 4854; b) B. Hedman, K. O. Hodgson, E. I. Solomon, *J. Am. Chem. Soc.* **1990**, *112*, 1643.

[21] a) R. K. Szilagyi, P. A. Bryngelson, M. J. Maroney, B. Hedman, K. O. Hodgson, E. I. Solomon, *J. Am. Chem. Soc.* **2004**, *126*, 3018; b) S. DeBeer George, M. Metz, R. K. Szilagyi, H. X. Wang, S. P. Cramer, Y. Lu, W. B. Tolman, B. Hedman, K. O. Hodgson, E. I. Solomon, *J. Am. Chem. Soc.* **2001**, *123*, 5757; c) E. Anxolabéhère-Mallart, T. Glaser, P. Frank, A. Aliverti, G. Zanetti, B. Hedman, K. O. Hodgson, E. I. Solomon, *J. Am. Chem. Soc.* **2001**, *123*, 5444; d) A. Dey, T. Glaser, J. J. G. Moura, R. H. Holm, B. Hedman, K. O. Hodgson, E. I. Solomon, *J. Am. Chem. Soc.* **2004**, *126*, 16868; e) T. Glaser, I Bertini, J. J. G. Moura, B. Hedman, K. O. Hodgson, E. I. Solomon, *J. Am. Chem. Soc.* **2001**, *123*, 4859.

[22] a) D. Herebian, K. Wieghardt, F. Neese, *J. Am. Chem. Soc.* **2003**, *125*, 10997; b) D. Herebian, E. Bothe, F. Neese, T. Weyhermüller, K. Wieghardt, *J. Am. Chem. Soc.* **2003**, *125*, 9116; c) P. Ghosh, E. Bill, T. Weyhermüller, F. Neese, K. Wieghardt, *J. Am. Chem. Soc.* **2003**, *125*, 1293.

[23] B. Hedman, P. Frank, S. F. Gheller, A. L. Roe, W. E. Newton, K. O. Hodgson, *J. Am. Chem. Soc.* **1988**, *110*, 3798.

[24] F. Neese, Orca—an ab initio, DFT and semiempirical Electronic Structure Package, Version 2.4, Revision 16, Max-Planck Institut für Bioanorganische Chemie, Mülheim (Germany), November **2004**.

[25] a) E. van Lenthe, j. G. Snijders, E. J. Baerends, *J. Chem. Phys.* **1996**, *105*, 6505; b) C. van Wüllen, *J. Chem. Phys.* **1998**, *109*, 392.

[26] J. H. van Lenthe, S. Faas, J. G. Snijders, *Chem. Phys. Lett.* **2000**, *328*, 107.

[27] a) A. D. Becke, *J. Chem. Phys.* **1986**, *84*, 4524; b) J. P. Perdew, *Phys. Rev. B* **1986**, *33*, 8522; c) F. Neese, G. Olbrich, *Chem. Phys. Lett.* **2002**, *362*, 170.

[28] a) S. Huzinaga, B. Miguel, *Chem. Phys. Lett.* **1990**, *175*, 289; b) S. Huzinaga, M. Klobukowski, *Chem. Phys. Lett.* **1993**, *212*, 260.

[29] a) A. Schäfer, H. Horn, R. Ahlrichs, *J. Chem. Phys.* **1992**, *97*, 2571; b) A. Schäfer, C. Huber, R. Ahlrichs, *J. Chem. Phys.* **1994**, *100*, 5289.

[30] A. Klamt, G. Schuurmann, *J. Chem. Soc. Perkin Trans. 2* **1993**, *2*, 799.

[31] R. Sarangi, N. Aboelella, K. Fujisawa, W. B. Tolman, B. Hedman, K. O. Hodgson, E. I. Solomon, *J. Am. Chem. Soc.* **2006**, *128*, 8286.

[32] X. Ribas, J. C. Dias, J. Morgado, K. Wurst, E. Molins, E. Ruiz, M. Almeida, J. Veciana, C. Rovira, *Chem. Eur. J.* **2004**, *10*, 1691.

[33] a) D. Herebian, E. Bothe, F. Neese, T. Weyhermüller, K. Wieghardt, *J. Am. Chem. Soc.* **2003**, *125*, 9116; b) D. Herebian, K. Wieghardt, F. Neese, *J. Am. Chem. Soc.* **2003**, *125*, 10997.

[34] a) K. Rüdenberg, *Rev. Mod. Phys.* **1962**, *34*, 326; b) M. J. Feinberg, K. Rüdenberg, E. L. Mehler, *Adv. Quantum Chem.* **1970**, *5*, 27; c) M. J. Feinberg, K. Rüdenberg, *J. Chem. Phys.* **1971**, *54*, 1495.

[35] A. L. Nivorozhkin, B. M. Segal, B. M. Kristin, S. A. Kates, B. Hedman, K. O. Hodgson, R. H. Holm, *Inorg. Chem.* **2000**, *39*, 2306.

[36] a) S. DeBeer George, L. Basumallick, R. K. Szilagyi, D. W. Randall, G. Michael, A. M. Nersissian, J. S. Valentine, B. Hedman, K. O. Hodgson, E. I. Solomon, *J. Am. Chem. Soc.* **2003**, *125*, 11314; b) D. W. Randall, S. DeBeer George, P. L. Holland, B. Hedman, K. O. Hodgson, W. B. Tolman, E. I. Solomon, *J. Am. Chem. Soc.* **2000**, *122*, 11632; c) A. E. Palmer, D. W. Randall, F. Xu, E. I. Solomon, *J. Am. Chem. Soc.* **1999**, *121*, 7138; d) S. E. Shadle, J. E. Penner-Hahn, H. J. Schugar, B. Hedman, K. O. Hodgson, E. I. Solomon, *J. Am. Chem. Soc.* **1993**, *115*, 767; e) F. Neese, W. G. Zumft, W. E. Antholine, P. M. H. Kroneck, *J. Am. Chem. Soc.* **1996**, *118*, 8692; f) F. Neese, R. Kappl, W. G. Zumft, J. Hüttermann, P. M. H. Kroneck, *J. Biol. Inorg. Chem.* **1998**, *3*, 53; g) J. Farrar, F. Neese, P. Lappalainen, P. M. H. Kroneck, M. Saraste, W. G. Zumft, A. J. Thomson, *J. Am. Chem. Soc.* **1996**, *118*, 11501.

[37] R. Kapre, K. Ray, I Sylvestre, T. Weyhermüller, S. DeBeer George, F. Neese, K. Wieghardt, *Inorg. Chem.* **2006**, *45*, 3499.

Received: October 5, 2006
Published online: February 9, 2007

